



The effect of heat treatment on the performance and structure of carbon-supported Au–Pd catalysts for the direct synthesis of hydrogen peroxide

Jennifer K. Edwards^{a,*}, James Pritchard^a, Marco Piccinini^a, Greg Shaw^a, Qian He^b,
Albert F. Carley^a, Christopher J. Kiely^b, Graham J. Hutchings^{a,*}

^a Cardiff Catalysis Institute, School of Chemistry, Cardiff University, Main Building, Park Place, Cardiff CF10 3AT, UK

^b Department of Materials Science and Engineering, Lehigh University, 5 East Packer Avenue, Bethlehem, PA 18015-3195, USA

ARTICLE INFO

Article history:

Received 16 August 2011

Revised 2 May 2012

Accepted 24 May 2012

Available online 30 June 2012

Keywords:

Gold palladium nanoparticles
Hydrogen peroxide direct synthesis
Aberration-corrected microscopy

ABSTRACT

The direct synthesis of hydrogen peroxide using supported gold palladium catalysts prepared by incipient wetness impregnation is described and discussed. The effect of an acid pre-treatment step on the activated carbon support prior to the deposition of the metals, together with the effect of the calcination temperature, has been investigated. The acid pre-treated samples all show superior activity to those materials prepared with the omission of this acid pre-treatment stage. The calcination temperature affects both the re-usability and hydrogenation activity of the catalysts. Detailed characterisation using X-ray photoelectron spectroscopy and aberration-corrected scanning transmission electron microscopy is described. The enhanced activity is associated with a higher surface concentration of palladium in the acid pre-treated samples which is principally present as Pd²⁺. Calcination of the catalysts at 400 °C is required to achieve re-usable and stable catalysts, and this is associated with the morphology and dispersion of the metal nanoparticles. The surface ratio of Pd⁰/Pd²⁺ is found to be an important factor controlling the hydrogenation of hydrogen peroxide, and a series of controlled reduction and re-oxidation of a sample show how the Pd⁰/Pd²⁺ surface ratio can influence the relative rates of hydrogen peroxide synthesis and hydrogenation.

© 2012 Elsevier Inc. All rights reserved.

1. Introduction

Hydrogen peroxide is a valuable commodity chemical with a vast range of applications; of the more than 3 million tonnes of hydrogen peroxide produced annually, some 60% is used for the bleaching of wood and textiles [1]. In terms of oxidation chemistry, hydrogen peroxide has a very high active oxygen content, as well as an oxidation potential greater than that of KMnO₄ and Cl₂. Coupled with its inherently benign nature (H₂O being produced as the only side product) and the observation that it produces activated oxygen species under milder conditions than di-oxygen, H₂O₂ is an ideal oxidant for the production of bulk chemicals. By far the great majority of H₂O₂ is produced by an indirect process in which H₂ and O₂ are reacted separately and safely with an alkyl anthraquinone as a molecular vector for hydrogen [2,3]. The anthraquinone is sequentially hydrogenated and oxidised to yield H₂O₂. This process is economic only on a large scale and consequently produces concentrated H₂O₂ (up to 70 vol%), which is then transported to its point of use. Furthermore, although the process has been improved over many decades of operation, it is still not

completely efficient, which provides an opportunity for a new technology to be developed that can be used particularly for small-scale synthesis of H₂O₂ solutions at the dilution levels at which they are typically employed. The direct synthesis of hydrogen peroxide from molecular hydrogen and oxygen presents an attractive alternative to the current industrial process, and much work has been focussed on the formulation of catalysts that are both active and selective for this reaction.

For a catalyst to be viable for the direct synthesis reaction, it must exhibit high H₂ selectivity towards H₂O₂, and if the H₂O₂ produced during the direct synthesis process is to be subsequently used as an oxidant, the H₂O₂ solution must be free of the halide and acid additives that Pd catalysts typically require in the reaction medium in order to achieve adequate activity and selectivity [4–10]. The addition of Au into Pd catalysts was shown to provide materials that were extremely active for the direct synthesis process [11–13] and yet still worked well in the absence of any acid and halide stabilisers. For a 2.5 wt% Au–2.5 wt% Pd/TiO₂ catalyst, a H₂ selectivity of >60% was observed, along with an activity of 64 mol_{H₂O₂} kg_{cat}⁻¹ h⁻¹ [11]. More recently, we demonstrated that an acid pre-treatment of the catalyst support (TiO₂ or activated carbon) further significantly increased the activity and selectivity of the resulting supported AuPd catalyst [14,15]. Most importantly, these acid-treated carbon-supported bimetallic catalysts were found to

* Corresponding authors.

E-mail addresses: edwardsjk@cf.ac.uk (J.K. Edwards), hutch@cardiff.ac.uk (G.J. Hutchings).

be inactive for the hydrogenation reaction (Scheme 1), which consumes H_2 non-selectively to form water [15]. This acid pre-treatment methodology was then applied to TiO_2 , and although some hydrogenation activity was observed over the acid-treated AuPd catalyst, it was considerably decreased as compared to that of the corresponding untreated catalyst [14]. Interestingly, for the 2.5 wt% Au–2.5 wt% Pd/ TiO_2 catalyst, a calcination temperature of 400 °C is required in order to generate a stable material and maintain a H_2O_2 synthesis activity of $64 \text{ mol}_{H_2O_2} \text{ kg}_{cat}^{-1} \text{ h}^{-1}$ on subsequent re-use [11]. In contrast, when the dried-only (25 °C) material was evaluated for hydrogen peroxide synthesis, the measured activity was much higher, at $202 \text{ mol}_{H_2O_2} \text{ kg}_{cat}^{-1} \text{ h}^{-1}$. Unfortunately, the activity of this material is not maintained on further use and deactivates as Au and Pd progressively leach from the catalyst. It is also important to follow the particular impregnation method precisely as slight deviations can also affect the resulting synthesis activity of a catalyst. For instance, the dissolution of Au and Pd precursors in excess water prior to the drying step generates a more active AuPd/ TiO_2 catalyst after subsequent calcination at 400 °C [16]. However, although more active, this latter material is, interestingly, unstable despite the heat treatment at 400 °C. Scanning transmission electron microscopy (STEM) analysis of the catalyst showed little or no alloying between Au and Pd in this latter material, whereas previously a well-defined core-shell morphology was shown to exist [11]. It is crucial, therefore, that the preparation conditions, and particularly the heat treatment during the fabrication of the supported AuPd catalysts, is carefully controlled in order to obtain the most effective catalyst for the direct synthesis of H_2O_2 . In this paper, we extend these studies and show that the heat treatment regimen of the acid pre-treated 2.5 wt% Au–2.5 wt% Pd/activated carbon catalyst is of fundamental importance in obtaining materials that both do not hydrogenate H_2O_2 and are also fully re-usable.

2. Experimental

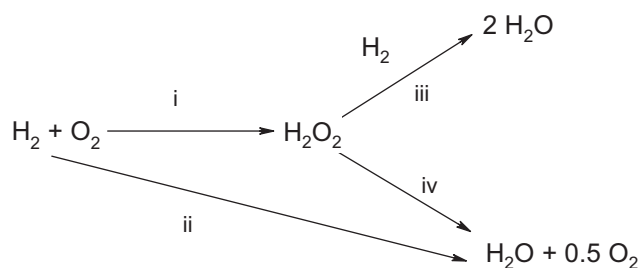
2.1. Catalyst preparation

Supported catalysts were prepared by incipient wetness impregnation of activated carbon (Aldrich G60) with aqueous solutions of $PdCl_2$ (Johnson Matthey) and/or $H AuCl_4 \cdot 3H_2O$ (Johnson Matthey) as previously described [15]. The catalyst was dried (120 °C, 16 h) and then portions of the material (0.2 g) were calcined at different temperatures in the range 200–400 °C for 3 h. Two sets of supports were used: the activated carbon as-received, and the carbon was after being subjected to a pre-treatment of dilute HNO_3 in water (2%) for 3 h at ambient temperature, with stirring. The precise details of this acid pre-treatment have been given previously [15].

2.2. Direct synthesis of H_2O_2

Caution: These experiments involve high pressures.

The catalysts were evaluated for the direct synthesis of hydrogen peroxide in a stainless steel autoclave (Parr Instruments) with a



Scheme 1. Potential reactions that can occur in the direct synthesis reaction: (i) H_2O_2 synthesis, (ii) competing direct H_2O synthesis, (iii) hydrogenation of H_2O_2 , and (iv) decomposition of H_2O_2 .

nominal volume of 100 ml and a maximum working pressure of 14 MPa. The autoclave was equipped with an overhead stirrer (0–2000 rpm) and provision for measurement of temperature and pressure. For the standard reaction conditions we have employed previously, the autoclave was charged with the catalyst (0.01 g), solvent (5.6 g MeOH and 2.9 g H_2O), purged three times with 5% H_2/CO_2 (0.7 MPa) and then filled with 5% H_2/CO_2 and 25% O_2/CO_2 to give a hydrogen to oxygen ratio of 1:2 at a total pressure of 4.0 MPa. Stirring (1200 rpm) was commenced on reaching the desired temperature (2 °C), and experiments were carried out for 30 min. The H_2O_2 yield was determined by titration of aliquots of the final filtered solution with acidified $Ce(SO_4)_2$ ($7 \times 10^{-3} \text{ mol dm}^{-3}$). The $Ce(SO_4)_2$ solutions were standardised against $(NH_4)_2Fe(SO_4)_2 \cdot 6H_2O$ using ferroin as indicator.

2.3. Hydrogenation of H_2O_2

Hydrogenation experiments were carried out as outlined above, but in the absence of 25% O_2/CO_2 in the gas stream and in the presence of 4 wt% H_2O_2 in the solvent (5.6 g methanol, 2.22 g H_2O , 0.68 g 50 wt% H_2O_2). The decrease in H_2O_2 concentration (determined from measurements made before and after reaction) is attributed to the combined hydrogenation and decomposition of H_2O_2 .

2.4. Catalyst characterisation

Temperature-programmed reduction was performed on a Thermo TPDRO utilising TCD detection. A sample of the fresh carbon and acid pre-treated carbon (0.1 g) was pre-treated at 120 °C with argon for 3 h. Following this, helium was flowed over the sample (20 ml min^{-1}) using a heating ramp of 5 °C min^{-1} until a maximum temperature of 1000 °C was reached. The gases evolved were monitored by an online thermal conductivity detector.

XPS measurements were made on a Kratos Axis Ultra DLD spectrometer using monochromatic Al $K\alpha$ radiation (120 W source power). An analyser pass energy of 160 eV was used for survey scans, whilst 40 eV was employed for detailed regional scans. Samples were mounted using double-sided adhesive tape, and binding energies were referenced to the C(1s) binding energy of adventitious carbon contamination taken to be 284.7 eV.

Thermogravimetric analysis was performed on a Setaram TG-DTA. A sample of fresh carbon and acid pre-treated carbon (30 mg) was placed in an aluminium crucible and heated to 350 °C at a ramp rate of 5 °C min^{-1} under a nitrogen atmosphere. Mass variation, temperature and heat flow were measured using a microbalance.

Samples for TEM and STEM analysis were prepared by dispersing the dry catalyst powder onto a holey carbon film supported by a 300 mesh copper TEM grid. Samples were first subjected to bright-field (BF) diffraction contrast imaging and X-ray energy-dispersive spectrometry (XEDS) in a JEOL 2000FX TEM operating at 200 kV. They were further characterised in a JEOL 2200 FS STEM instrument operating at 200 kV and equipped with a CEOS probe corrector, using high-angle annular dark field (HAADF) imaging in order to detect any highly dispersed metallic species.

3. Results and discussion

3.1. Direct synthesis and hydrogenation of H_2O_2

A series of Au, Pd and Au–Pd catalysts supported on activated carbon were prepared using wet impregnation. The activated carbon was either used pre-treated with aqueous HNO_3 prior to impregnation with the metals or was used by treatment with

water in an analogous manner (i.e. treated without acid present) prior to deposition of the metals (this is referred to as untreated). The catalysts were calcined under static air at 200 °C, 300 °C and 400 °C. These catalysts were then used for the direct synthesis of H₂O₂ using our standard reaction conditions, and the data we generated are given in Table 1. As we observed previously for the titania-supported catalyst [11], the dried and uncalcined 2.5 wt% Au–2.5 wt% Pd/carbon (acid pre-treated) material showed the highest activity (212 mol_{H₂O₂} kg_{cat}⁻¹ h⁻¹) for the direct synthesis reaction (Table 1). When the activity of the used catalyst was evaluated, a decrease in activity of ~50% to 101 mol_{H₂O₂} kg_{cat}⁻¹ h⁻¹ was observed. Increasing the temperature of calcination (200–300 °C) resulted in a decreased synthesis activity; however, the used material, whilst still unstable, retains more of its initial activity on re-use (~70% when calcined at 300 °C). When calcined at 400 °C, the material has a specific activity of 160 mol_{H₂O₂} kg_{cat}⁻¹ h⁻¹ on both first and second use. The hydrogenation activity of this same set of materials was determined (Table 1) and was also found to be dependant on calcination temperature. The dried 120 °C material showed the highest hydrogenation rate of 736 mol_{H₂O₂} kg_{cat}⁻¹ h⁻¹, which corresponds to 36% of the total H₂O₂ being lost. However, increasing the calcination temperature decreases the hydrogenation rate, such that at 400 °C the catalyst exhibits no hydrogenation activity. In order to investigate how temperature-specific this effect is, a small batch of the dried material was calcined at 350 °C (i.e. between 300 and 400 °C) and was still found to hydrogenate H₂O₂ (hydrogenation rate 279 mol_{H₂O₂} kg_{cat}⁻¹ h⁻¹).

We previously showed [15] that the non-acid pre-treated analogue of this catalyst does hydrogenate H₂O₂ when calcined at 400 °C and has a lower overall H₂O₂ synthesis rate (110 mol_{H₂O₂} kg_{cat}⁻¹ h⁻¹) than the acid pre-treated catalyst. For comparison, the same calcination series was prepared for the catalysts prepared on fresh activated carbon, and the H₂O₂ synthesis and hydrogenation rates were measured (Table 2). Interestingly, this material is not as sensitive to the precise calcination treatment as its acid pre-treated counterpart. The dried material has an activity of 130 mol_{H₂O₂} kg_{cat}⁻¹ h⁻¹, whereas the catalyst calcined at 400 °C has an activity of 110 mol_{H₂O₂} kg_{cat}⁻¹ h⁻¹. The dried-only material also retains much more activity on subsequent use, as do the catalysts calcined at 200 °C and 300 °C. However, a calcination temperature of 400 °C is required to retain the activity of 110 mol_{H₂O₂} kg_{cat}⁻¹ h⁻¹ upon subsequent re-use. The hydrogenation activity of the dried untreated material is similar to that of the acid pre-treated sample up to calcination temperatures of 300 °C. Crucially, the hydrogenation rate of the material calcined at 400 °C is still maintained at 120 mol_{H₂O₂} kg_{cat}⁻¹ h⁻¹ as compared with a hydrogenation rate of 0 mol_{H₂O₂} kg_{cat}⁻¹ h⁻¹ for the corresponding acid pre-treated material.

3.2. Characterisation of the carbon support

3.2.1. Thermogravimetric analysis

The TGA analysis of the as received carbon (Fig. S1) and the acid pre-treated carbon (Fig. S2) show no differences between the

supports, with both materials showing equal amounts of H₂O loss (2.7%).

3.2.2. X-ray photoelectron spectroscopy

The bare acid pre-treated and untreated supports were analysed by XPS in an attempt to determine the origin of the different activities observed for the supported AuPd catalysts. The C(1s) and O(1s) spectra are shown in Figs. 1 and 2 for the 120 °C supports before and after TGA analysis, indicating the functionality of the carbon remains the same on both carbons after thermal treatment up to 350 °C. Somewhat surprisingly, no significant differences were observed between the untreated and acid pre-treated materials.

3.2.3. Temperature-programmed desorption

The temperature-programmed desorption (TPD) profiles presented in Fig. 3 for the untreated and acid pre-treated carbon supports show a clear difference in surface oxygen functionality related to the desorption of CO₂. The signal at 180 °C for the acid pre-treated sample implies an increase in the number of surface carboxylic acid (and hence –OH) groups [17–19]. The peak broadening, extending from approximately 240–350 °C, suggests a further increase, albeit slight, in the number density of carboxylic groups as the temperature of the desorption correlates with acid strength. Minor peak features in the same region for the untreated carbon suggest that a baseline number of carboxylic groups exist prior to any treatment and that the acid pre-treatment is therefore effectively increasing the number of carboxylic acid surface groups [17,20].

In both desorption profiles, an increased response is observed at temperatures in the 400–700 °C range. This is consistent with the desorption of carboxylic anhydrides and lactone/ether groups occurring at higher temperature. However, the desorption events observed at 700 °C can be complicated by CO desorption, as well as desorption of CO₂ originating from the acid functional groups.

3.3. Characterisation of the carbon-supported AuPd catalysts

3.3.1. X-Ray photoelectron spectroscopy

Au–Pd catalysts supported on the untreated and acid pre-treated carbon, which had been calcined at a variety of different temperatures, were analysed by XPS. In our initial study [15], we noted that there were no differences in the N region of the XPS for the acid pre-treated and the untreated samples, so we have therefore concentrated on other spectral regions in this work. The Pd(3d) spectra for the two series of catalysts are shown in Fig. 4 (untreated support) and Fig. 5 (acid pre-treated support). Table 3 shows the quantified XPS data and in particular the molar surface Pd/Au ratios. For samples on the untreated carbon support, the Pd/Au ratio is relatively constant as a function of calcination temperature, having a value in the range 1.0–1.4; the molar ratio for a nominal 2.5 wt% Au–2.5 wt% Pd loading is 1.8. In contrast, the ratio for the catalysts supported on the acid pre-treated carbon show a significant increase in the Pd/Au ratio with calcination temperature. This

Table 1

H₂O₂ synthesis activity of 2.5 wt% Au–2.5 wt% Pd/carbon catalysts (pre-treated with 2% HNO₃) that were calcined at different temperatures.

Heat treatment ^a	Productivity (mol _{H₂O₂} kg _{cat} ⁻¹ h ⁻¹) ^b		Hydrogenation (mol _{H₂O₂} kg _{cat} ⁻¹ h ⁻¹)
	Initial activity	Re-use activity ^c	
Dried 120 °C	212	101	736
Calcined 200 °C	180	106	617
Calcined 300 °C	174	124	546
Calcined 400 °C	160	160	0

^a Metal loadings are denoted as mass fractions. All catalysts were dried in air at 120 °C and then calcined for 3 h in static air as indicated.

^b Reaction conditions: catalyst (10 mg), 2.9 MPa H₂ (5% volume fraction)/CO₂ 1.1 MPa O₂ (25% volume fraction)/CO₂, 2 °C, 0.5 h, methanol/water as solvent.

^c Activity on re-use determined by recovering catalyst after first synthesis, drying in air at RT, and then re-assessing activity under standard reaction conditions.

Table 2

H₂O₂ hydrogenation activity of 2.5 wt% Au–2.5 wt% Pd/carbon catalysts (untreated with 2% HNO₃) that were calcined at different temperatures.

Heat treatment ^a	Productivity (mol _{H₂O₂} kg _{cat} ⁻¹ h ⁻¹) ^b		Hydrogenation (mol _{H₂O₂} kg _{cat} ⁻¹ h ⁻¹)
	Initial activity	Re-use activity ^c	
Dried 120 °C	120	79	729
Calcined 200 °C	120	105	707
Calcined 300 °C	130	108	499
Calcined 400 °C	110	110	120

^a Metal loadings are denoted as mass fractions. All catalysts dried in air 120 °C then calcined for 3 h in static air as indicated.

^b Reaction conditions: catalyst (10 mg), 2.9 MPa H₂ (5% volume fraction)/CO₂, 1.1 MPa O₂ (25% volume fraction)/CO₂, 2 °C, 0.5 h, methanol/water as solvent.

^c Activity on re-use determined by recovering catalyst after first synthesis, drying in air at RT and then re-assessing activity under standard reaction conditions.

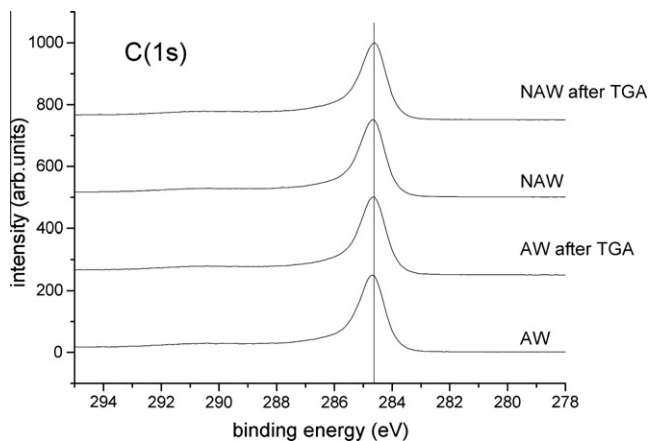


Fig. 1. C(1s) XPS spectra observed for untreated (denoted NAW) and acid pre-treated (denoted AW) C supports before and after thermogravimetric analysis under nitrogen atmosphere.

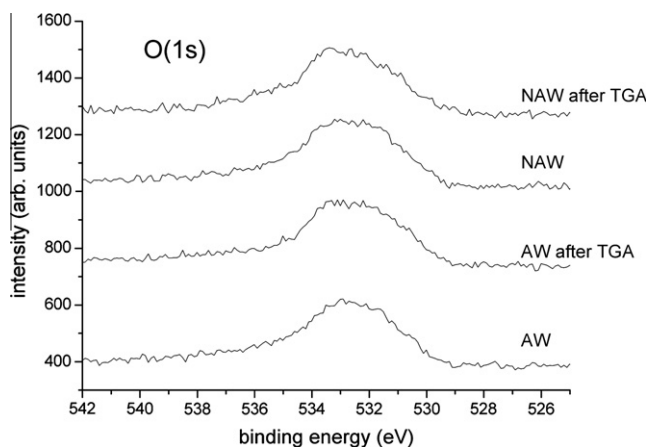


Fig. 2. O(1s) XPS spectra observed for untreated (denoted NAW) and acid pre-treated (denoted AW) C supports before and after thermogravimetric analysis under nitrogen atmosphere.

observation could in principle reflect the formation of core–shell type particles although the detailed electron microscopy analysis presented later shows that this is not the case. Hence, we consider that the variation in Pd/Au ratio can be explained by changes in the relative sizes of the Pd and Au nanoparticles. The catalysts prepared on the untreated support exhibit both Pd²⁺ and Pd⁰ species, the relative proportions of which change little with calcination temperature (Table 3). In contrast, Pd²⁺ species are predominant (>90%) on the catalysts prepared on the acid pre-treated support, for all calcination temperatures. This clearly represents an important difference between the two sets of samples, with the elec-

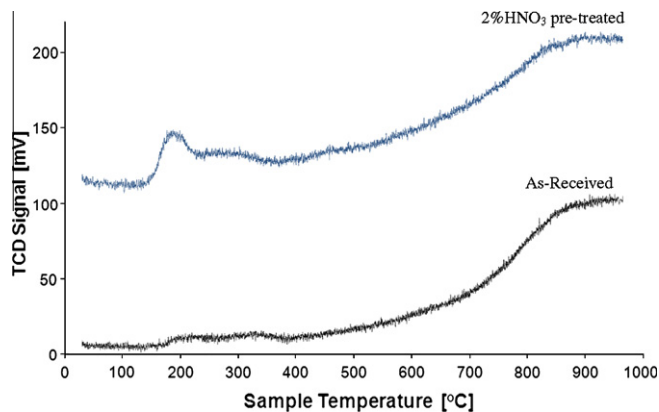


Fig. 3. Temperature-programmed desorption profiles for 2% HNO₃ pre-treated (blue) and untreated (black) C supports only. (For interpretation of the references to colour in this figure legend, the reader is referred to the web version of this article.)

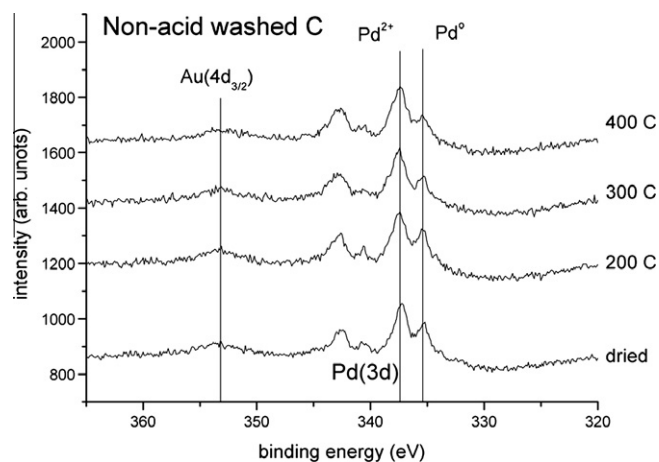


Fig. 4. Pd(3d) spectra observed for the 2.5 wt% Au–2.5 wt% Pd catalysts supported on untreated carbon and calcined at the temperatures indicated.

tronic state of the highly dispersed Pd being modified as a consequence of the acid pre-treatment of the support.

The Cl(2p) spectra for the catalysts prepared on the untreated and acid pre-treated carbon are shown in Figs. 6 and 7 respectively. In this case, the Cl signal is a residue from the two metal precursors used to prepare the catalysts. At first sight, the sets of Cl(2p) spectra clearly involve more than one Cl(2p) doublet. Closer inspection reveals that the Cl(2p) spectra from the catalysts prepared on the as-received carbon comprise two (spin–orbit) 2p doublets, the relative intensities of which change with calcination temperature. However, for the acid pre-treated catalysts, three doublets are

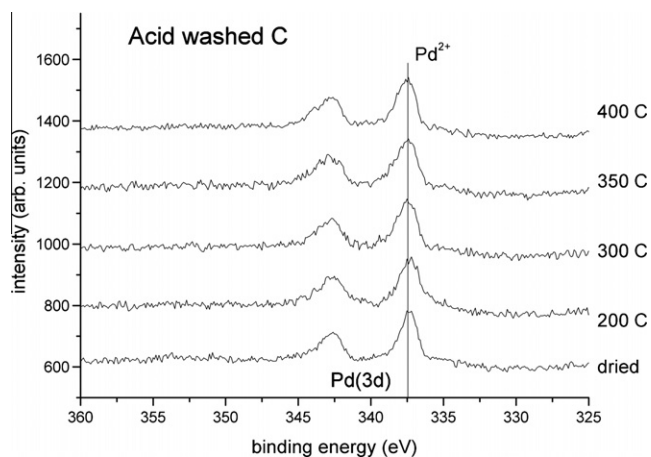


Fig. 5. Pd(3d) spectra observed for the 2.5 wt% Au–2.5 wt% Pd catalysts supported on acid pre-treated carbon and calcined at the temperatures indicated.

Table 3

Quantified XP data for the 2.5 wt% Au–2.5 wt% Pd/carbon catalysts; data are included for the both the untreated and acid-treated supports.

Molar ratios	Pd/Au	(Pd + Au)/C ($\times 100$)	Cl/C ($\times 100$)	Pd ²⁺ (%)
<i>Acid pre-treated (°C)</i>				
Dried 120 °C	2.7	0.44	0.71	>90
200 °C	3.8	0.45	0.61	>90
300 °C	4.3	0.46	0.51	>90
350 °C	4.1	0.41	0.44	>90
400 °C	4.2	0.50	0.42	>90
<i>Untreated (°C)</i>				
Dried 120 °C	1.0	0.70	0.61	60
200 °C	1.1	0.66	0.51	57
300 °C	1.3	0.61	0.50	69
400 °C	1.4	0.63	0.44	68

needed to describe the spectra (Fig. 7). For each support, the higher binding energy doublet (corresponding to a more ionic, negatively charged Cl^{x-} species) dominates after calcination at 400 °C. Table 4 shows the quantified curve-fitted XPS data for the untreated samples presented in Fig. 6.

3.3.2. Electron microscopy characterisation

The unused catalysts were studied using transmission electron microscopy in order to determine the Au and Pd distribution on the

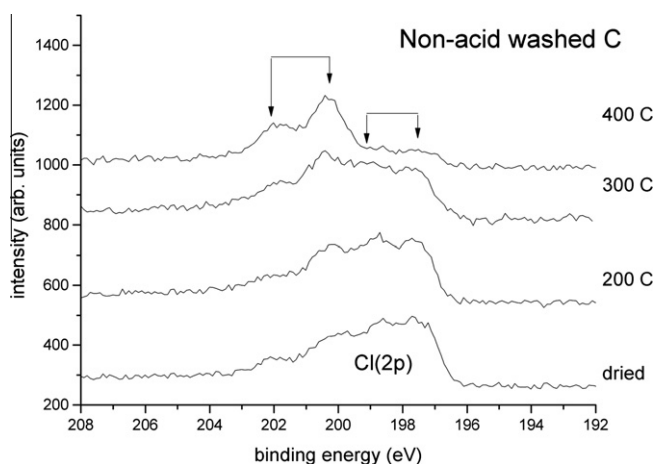


Fig. 6. Cl(2p) spectra observed for the 2.5 wt% Au–2.5 wt% Pd catalysts supported on non-pre-treated carbon and calcined at the temperatures indicated.

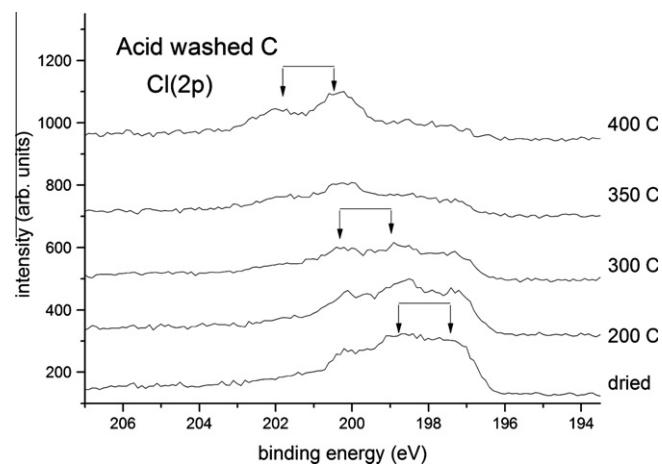


Fig. 7. Cl(2p) spectra observed for the 2.5 wt% Au–2.5 wt% Pd catalysts supported on acid pre-treated carbon and calcined at the temperatures indicated.

support as a function of calcination temperature. Representative bright-field TEM micrographs from acid pre-treated Au–Pd/C catalysts heat treated at different temperatures (dried at 120 °C, calcined at 200 °C, 300 °C and 400 °C) are shown in Fig. 8. Occasional metallic particles between 30 and 100 nm in size were found in all samples, whilst the majority of the activated carbon support appeared devoid of metal particles in the bright-field TEM images. Energy-dispersive X-ray spectra that were acquired from the areas with and without visible particles are shown in Fig. 9. Both Au and Pd were detected from the larger metallic particles (with the Au signal being pre-dominant), whereas only a Pd signal was detected in those support areas that were apparently devoid of metal particles. This suggested that the Au component of the catalysts was incorporated mainly in the nanoparticles, whereas most of the Pd existed in a highly dispersed form that cannot be seen using regular BF-TEM imaging.

Fig. 10 shows representative STEM–HAADF images of the acid pre-treated Au–Pd/C catalysts that had been calcined at various temperatures. As expected, in all the samples, highly dispersed Pd metal species, namely sub-nm clusters and single atoms, were found everywhere on the activated carbon support. In comparison with the sample dried at 120 °C, the population of sub-nm clusters seemed to get progressively lower as the calcination temperature was increased for this set of acid pre-treated samples. The calcination process appears to aid in dispersing the sub-nm clusters into dispersed atomically species. However, the differences between the morphology of samples with different calcination temperatures were rather subtle.

Representative STEM–HAADF images taken from the Au–Pd/C prepared on the untreated are shown in Fig. 11. They appeared very similar to their corresponding acid pre-treated counterparts (Fig. 10), indicating that the acid pre-treatment does not massively affect the morphology or distribution of the metallic species in these catalysts. A similar trend was noted as for the acid pre-treated

Table 4

Quantified curve-fitted data for the Cl(2p) spectra recorded for the catalysts prepared on the untreated C support (see Fig. 3).

Treatment	Binding energy (eV)		Split (eV)	% conc	
	#1	#2		#1	#2
Dried 120 °C	197.7	200.4	2.7	73	27
Calcined 200 °C	197.8	200.4	2.6	74	26
Calcined 300 °C	198.1	200.5	2.4	65	35
Calcined 400 °C	197.7	200.4	2.7	26	74

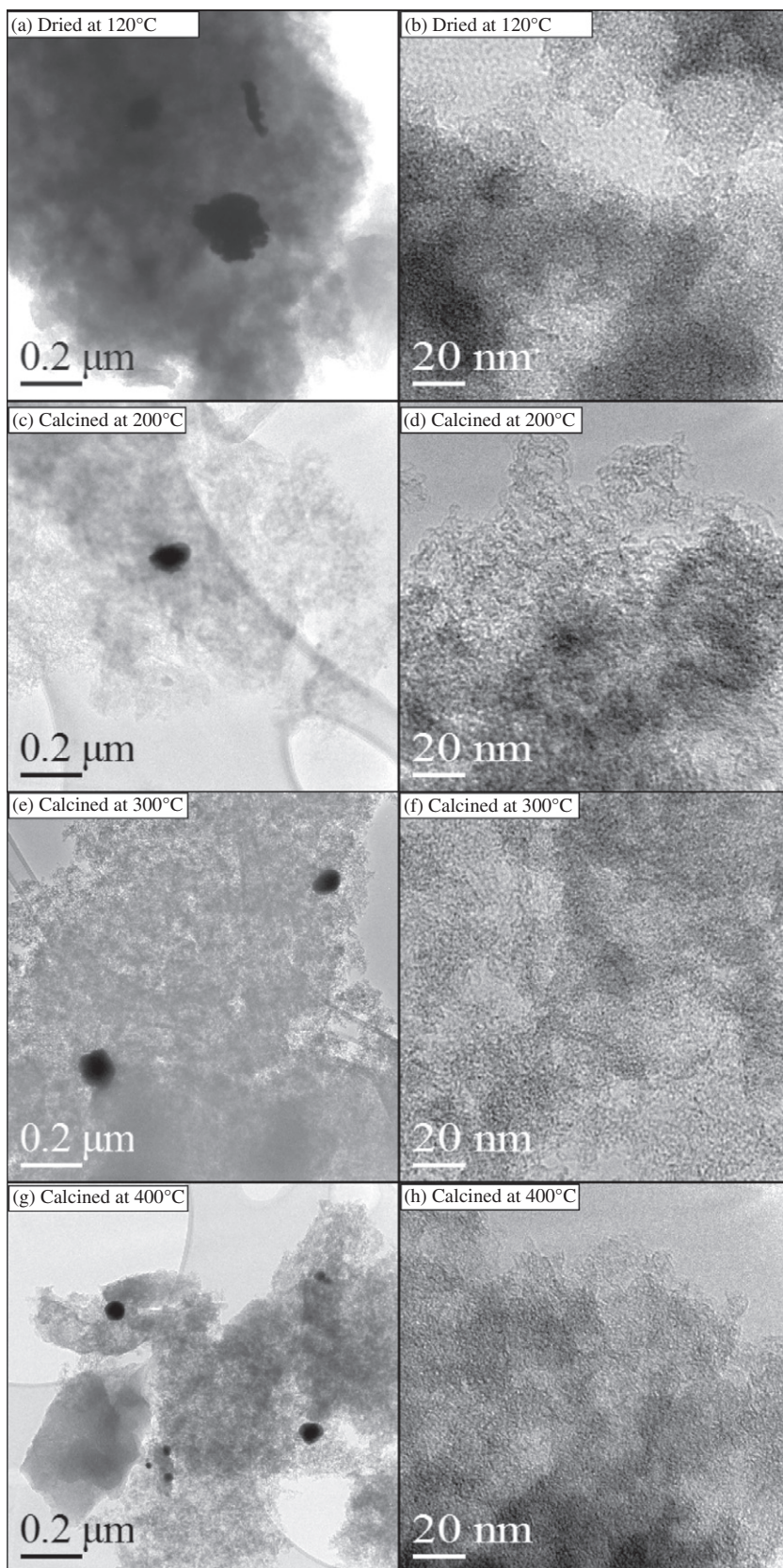


Fig. 8. Representative BF-TEM images of acid pre-treated AuPd/C catalysts calcined at different temperatures. (a and b) dried only at 120 °C; (c and d) calcined at 200 °C; (e and f) calcined at 300 °C; (g and h) calcined at 400 °C, showing the larger metallic nanoparticles and the carbon support.

materials, in that the population density of sub-nm Pd species decreased with increasing calcination temperature, compared to the sample dried at 120 °C.

As a baseline for this aberration-corrected microscopy study of the highly dispersed species in the AuPd/C samples, Fig. 12 shows representative STEM–HAADF images of the monometallic Au/C and

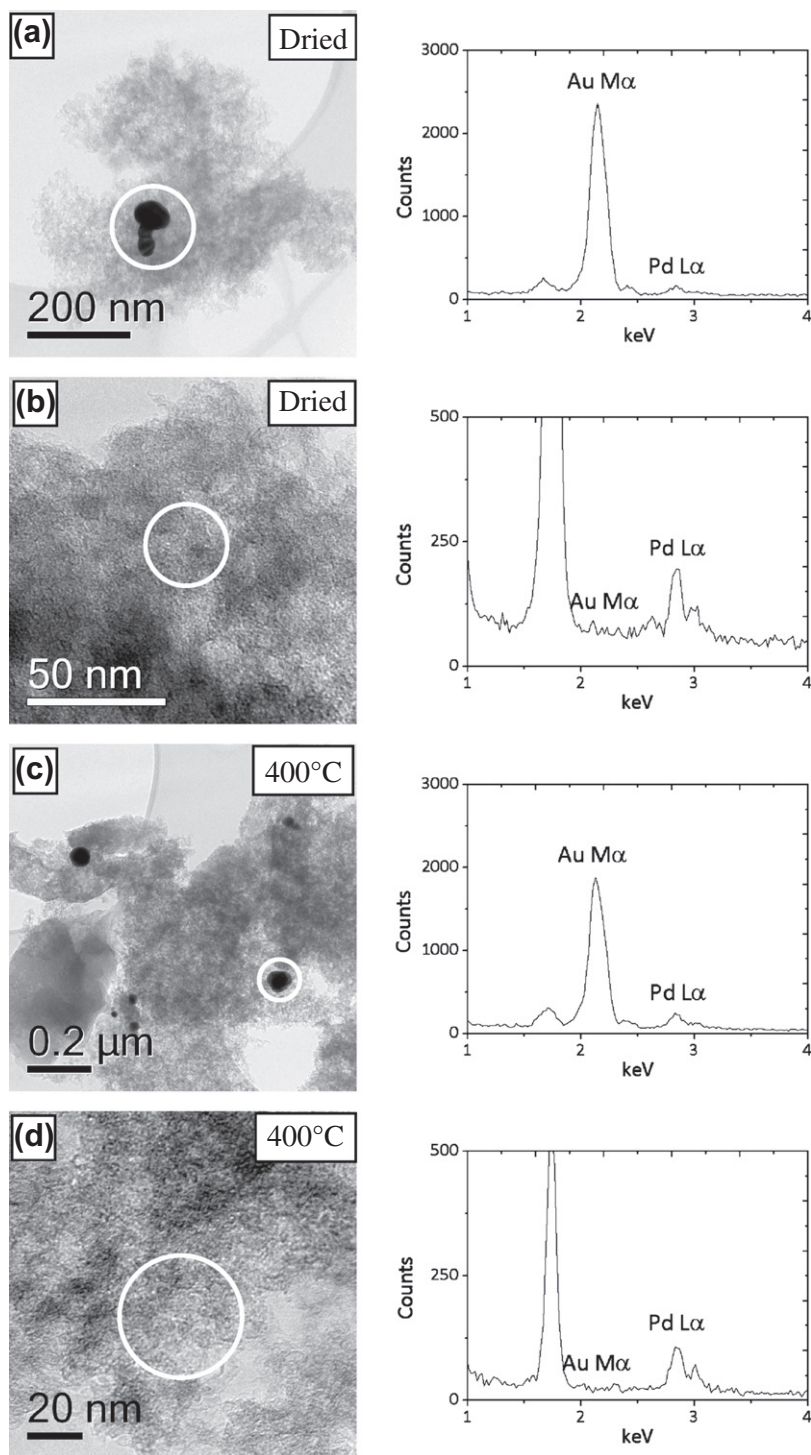


Fig. 9. Energy-dispersive X-ray spectra of acid pre-treated AuPd/C catalysts: (a) particle – dried only, (b) support – dried only, (c) particle – calcined at 400 °C, and (d) support – calcined at 400 °C. The white circles indicate the areas from where the XEDS spectra were acquired. The unlabelled peak Si K α at 1.74 keV is a fluorescence artefact from the Si(Li) X-ray detector, the intensity of which depends on the exact conditions (e.g. live-time) used during spectrum acquisition.

Pd/C catalysts, calcined at 400 °C. In the Pd/C sample, occasional nanoparticles (not shown), and numerous sub-nm Pd clusters and isolated Pd atoms were found in both the untreated and acid pre-treated samples, exhibiting a similar density to those found in their bi-metallic counterparts. For the Au/C sample, nanoparticles (not shown) and only a small fraction of isolated Au atoms were seen, but the number density of these isolated atoms was much lower than that found in the AuPd/C samples. We are unable

to directly determine the chemical identity of the sub-nm species and isolated atoms in the AuPd/C bimetallic system using atomic level Z-contrast measurements, due to the rough nature of the support, which leads to complicating height variations between neighbouring metallic species. However, our studies on the mono-metallic samples give us helpful clues as to what is probably occurring in the bimetallic AuPd/C system. They show that the Pd tends to be more highly dispersed using this particular impregnation

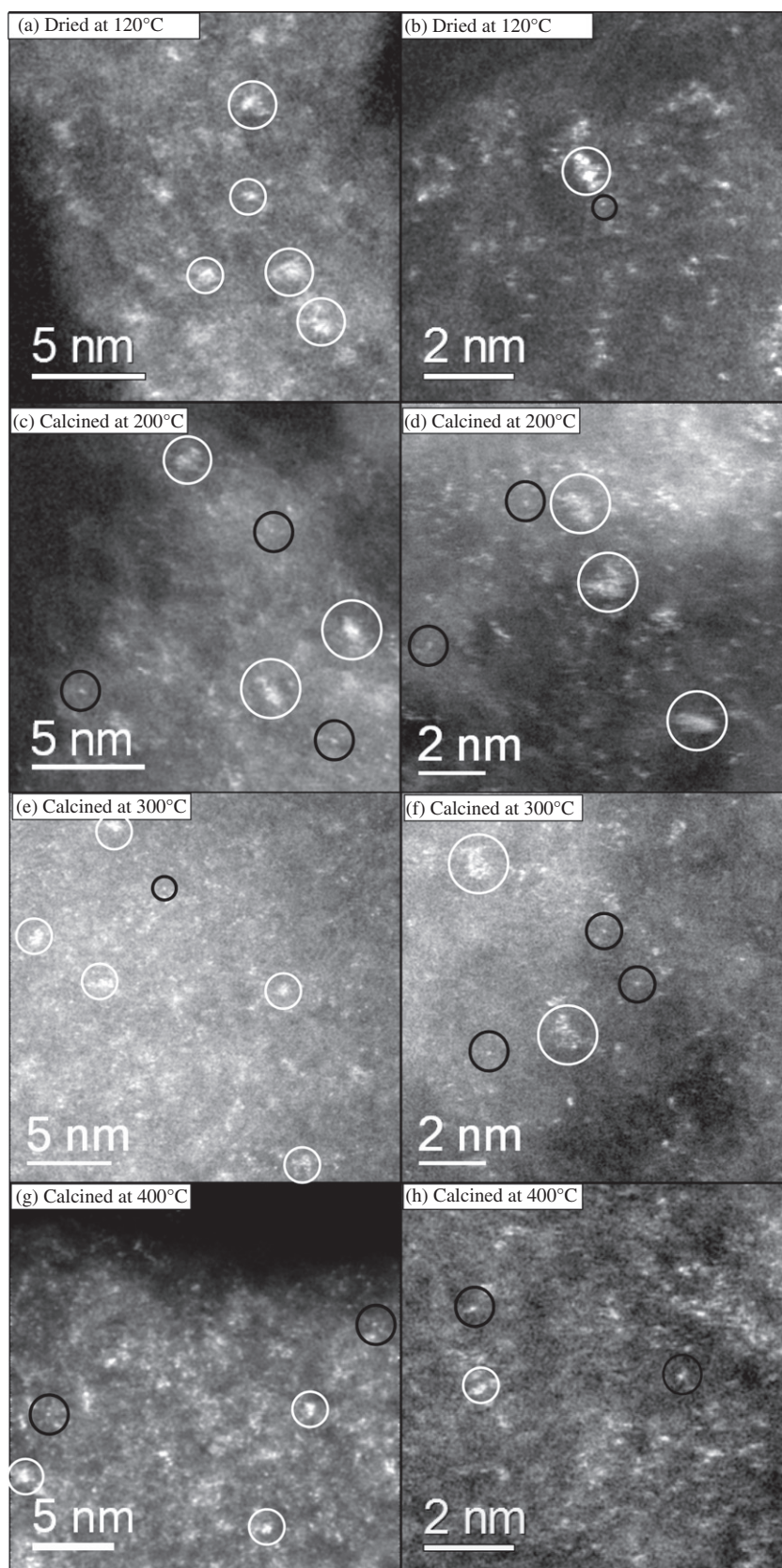


Fig. 10. Representative STEM-HAADF images of the acid pre-treated AuPd/C catalysts calcined at different temperatures. (a and b) dried only at 120 °C; (c and d) calcined at 200 °C; (e and f) calcined at 300 °C; (g and h) calcined at 400 °C. These micrographs show two types of highly dispersed metal species, namely sub-nm clusters (circled in white) and isolated atoms (circled in black). The number of those sub-nm clusters tends to decrease with increasing calcination temperature.

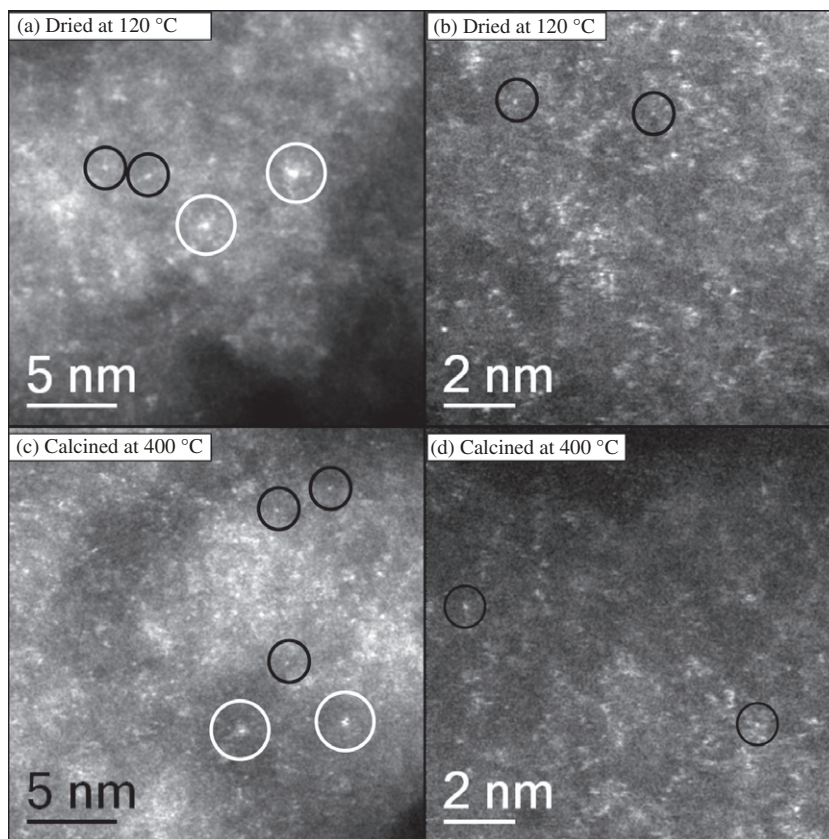


Fig. 11. STEM-HAADF images of untreated AuPd/C catalysts calcined at different temperatures. (a and b) dried only at 120 °C; (c and d) calcined at 400 °C; Sub-nm clusters (circled in white) and isolated atoms (circled in black) are shown in both samples. The morphologies are very similar to their acid pre-treated AuPd/C counterparts.

route, but that there is most likely a very dilute concentration of atomically dispersed Au atoms intermixed within the atomically dispersed Pd species in the bimetallic system.

In summary, electron microscopy studies have shown that the untreated and acid-treated Au–Pd/C samples calcined at 400 °C contain Au-rich nanoparticles and a highly dispersed coverage of atomic and cluster-like Pd species, intermixed with a small amount of atomically dispersed Au. The calcination treatment appears to improve the overall metal dispersion, but the acid pre-treatment of the support does not seem to affect the morphology or dispersion of the metallic species in the catalysts. This suggests that the change of oxidation state of the Pd to >90% cationic Pd observed by XPS (Table 3), associated with O^{2-} or Cl^- , is the most important distinguishing feature between the acid pre-treated and untreated samples.

3.4. Comments on the structure activity relationships

There are two key observations that we make through these sets of experiments, namely the effect of calcination temperature on catalyst stability and on the hydrogenation activity. Calcination at 400 °C is required for the supported AuPd/C catalysts to ensure they are stable during the hydrogen peroxide synthesis reaction. The acid pre-treatment has no influence on the optimal calcination temperature, although it is clear that the acid pre-treated samples are more affected by the calcination process with the dried material displaying a very high, but unstable, activity. Although a calcination treatment at 400 °C is required to achieve stability, it is clear that the acid pre-treated samples are always more active than their untreated counterparts. Yet the metal dispersion and morphologies are essentially identical and so cannot be responsible for this phenomenon. The detailed electron microscopy measurements show

that the calcination process improves the dispersion of the metals on the supports and this appears to be the key feature that governs the stability and re-usability of the catalysts, as well as the higher activity of the acid pre-treated samples at lower calcination temperatures. The XPS data additionally show that the nature of the Cl species changes significantly at calcination temperatures above 200 °C, in a way which is similar for both the acid pre-treated and untreated sets of samples, which seems to indicate that there is an electronic modification that is associated with improved re-usability.

The reason for the dramatic switching-off of the hydrogenation activity for the acid pre-treated sample calcined at 400 °C is much more difficult to explain at this time. A key difference is noted for the two supports before the metals are deposited, as the acid pre-treated carbon clearly shows an enhanced concentration of surface carboxylic acid functional groups. These species may play a key role in the enhanced activity we observe for the acid pre-treated catalysts and may aid the dispersion of the metals during preparation. XPS of the untreated set of samples shows that the surface comprises *ca.* 60–70% Pd^{2+} with 30–40% Pd^0 , whereas XPS of the acid pre-treated set of samples shows that at the limit of detection by this method, they comprise almost all Pd^{2+} on the surface with virtually no Pd^0 being detectable for all samples. This feature may be the underlying cause of the enhanced activity observed with the acid pre-treatment method. The amount of Pd^{2+} increased gradually with increasing calcination temperature for the water pre-treated samples (Table 3). It is therefore tempting to speculate that as the H_2O_2 hydrogenation activity of this set decreases with increased calcination temperature, that hydrogenation is associated with the presence of residual Pd^0 in the samples. However, the XPS spectra of the acid pre-treated set are very similar for all calcination temperatures, and with the exception of the 400 °C

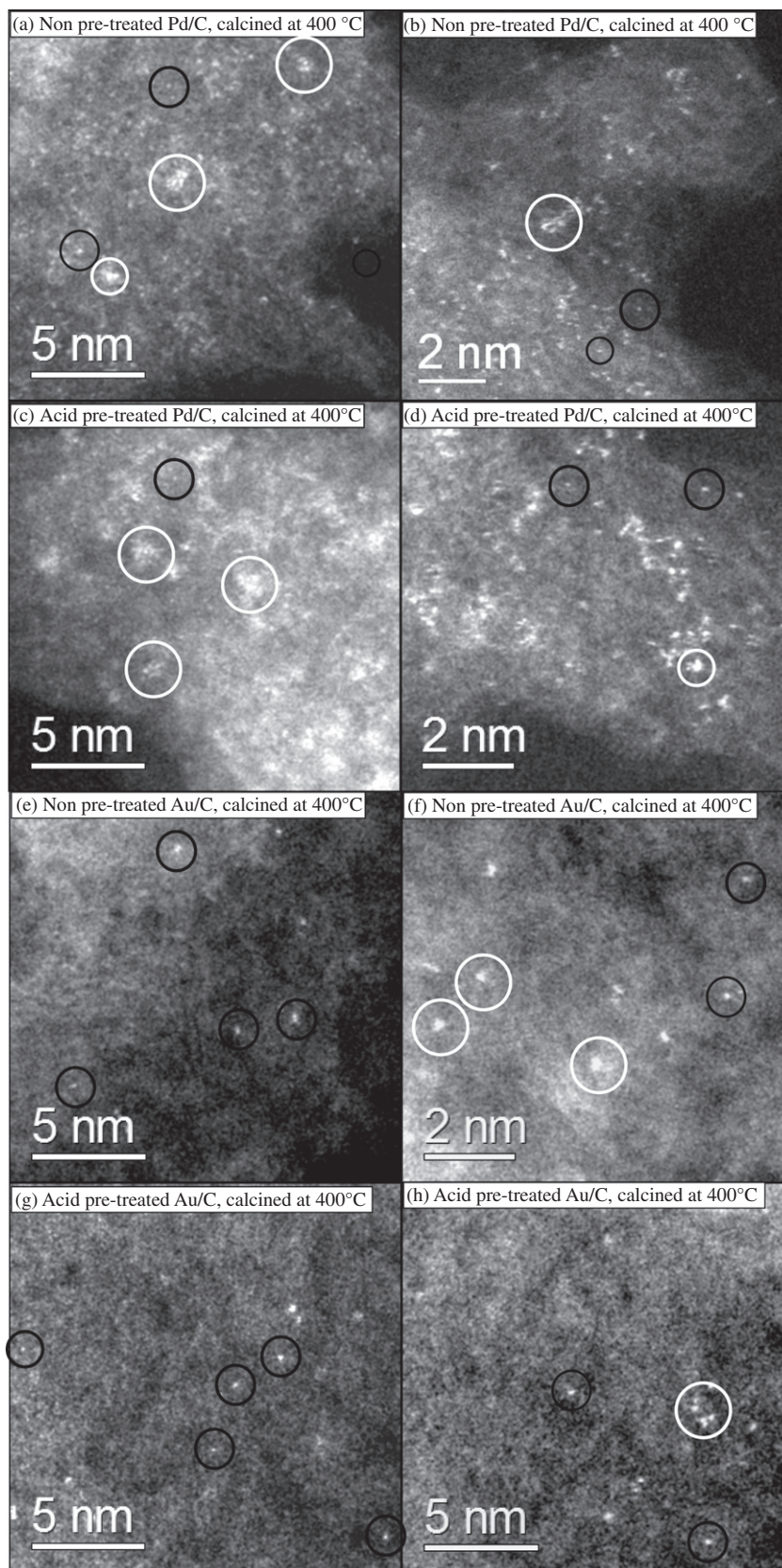


Fig. 12. STEM-HAADF images of the mono metallic Pd/C and Au/C catalysts calcined at 400 °C, both untreated (a, b, e, and f) and acid pre-treated (c, d, g, and h). Sub-nm Pd clusters (circled in white) and isolated Pd atoms (circled in black) were found in the Pd/C samples, and their population densities are similar to those noted for their bi-metallic AuPd/C counterparts. However, in the Au/C samples, only a low areal density of high intensity-isolated Au atoms was found in addition to the much larger gold nanoparticles.

Table 5
Effect of sequential reduction and oxidation on catalytic performance.

Entry	Heat treatment	H ₂ O ₂ productivity mol _{H₂O₂} kg _{cat} ⁻¹ h ⁻¹		H ₂ O ₂ hydrogenation mol _{H₂O₂} kg _{cat} ⁻¹ h ⁻¹ (%)
1	Initial catalyst	185		60
	Sample entry 1 + 5% H ₂ / Ar treatment			
	Temperature	Time		
2	100	1	176	72
3	110	2	173	86
4	150	2	141	126
5	200	2	80	286
	Sample entry 5 + O ₂ treatment			
6	100	3	116	180
7	200	3	126	0

calcined sample, they all hydrogenate H₂O₂. Hence, overall this evidence suggests that the Pd oxidation state may not be the determining factor controlling the hydrogenation activity. Another key observation is that the acid pre-treated samples all have much higher surface Pd/Au ratios as compared with the untreated samples. However, it is clear that this has little to do with the observed effects on hydrogenation activity or catalyst re-usability as there are no significant differences between the samples calcined at 200 and 400 °C in either set of samples. This enhanced surface Pd concentration, which is primarily present as Pd²⁺, may be another important parameter associated with the high activity of the acid pre-treated samples. Hence, with these samples we were unable to unequivocally identify the crucial feature responsible for

switching off the hydrogenation of H₂O₂, but there are definite indications that the surface oxidation state of Pd is an important factor.

We have therefore conducted an additional set of experiments that attempt to determine the origin of this effect. For these studies, we selected a sample prepared on the acid pre-treated carbon support that showed high activity, but had some residual hydrogenation activity. We achieved this through manipulation of the initial impregnation procedure as we have described previously [16]. We then subjected this sample to a series of reduction treatments and measured the catalytic performance of the reduced samples. The data are set out in Table 5, with entry 1 being the starting point for this sequence of experiments. We selected a sample with some hydrogenation activity for these experiments as we wanted to determine whether the hydrogenation could be either positively or negatively influenced by a reduction treatment. Reduction of this sample (Table 5, entries 2–5) shows that as the duration and temperature of the reduction step are increased, the production activity of H₂O₂ decreased and the hydrogenation of H₂O₂ increased markedly. We then took the sample from entry 5 and re-oxidised it. After re-oxidation, we observed the reverse trends on H₂O₂ formation and hydrogenation.

A series of STEM–HAADF images from this sequential set of reduction and oxidation samples are shown in Fig. 13. The starting point (Fig. 13a) was the 2.5 wt% Au–2.5 wt% Pd catalyst supported on acid pre-treated carbon that had been calcined at 400 °C for 3 h, which showed predominantly atomically dispersed Pd species intermixed with a small number of Au atoms (as noted previously in Fig. 10g and h). When this sample was heated in O₂ for 3 h (Fig. 13b), there was no observable change in the atomic dispersion of Pd and Au. Conversely, when the starting sample was reduced in

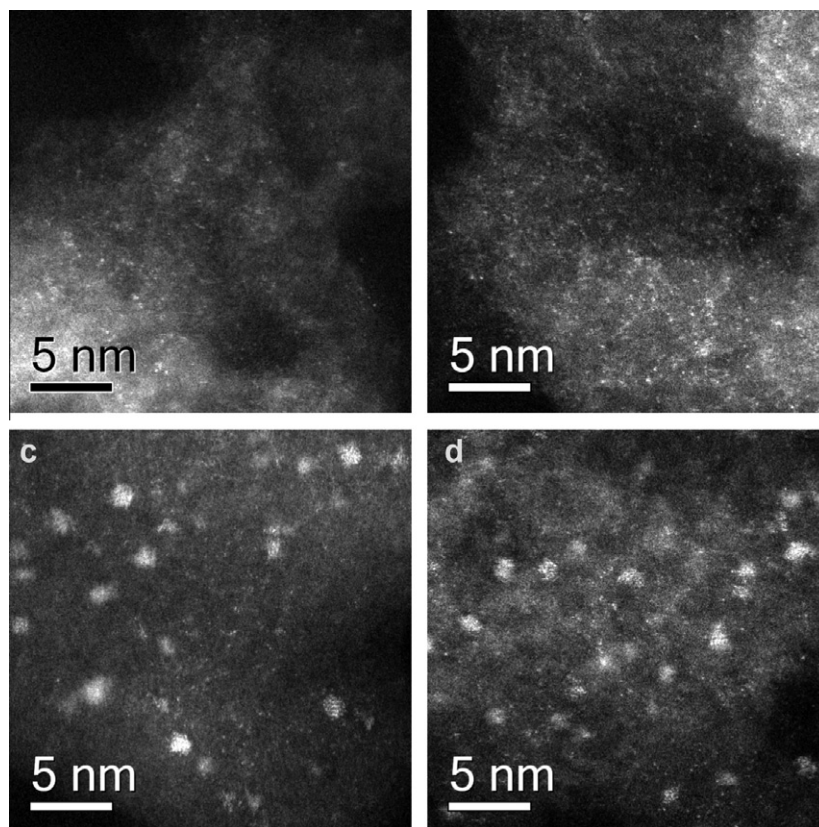


Fig. 13. STEM HAADF images of the 2.5 wt% Au–2.5 wt% Pd catalysts supported on acid pre-treated carbon with sequential reduction and oxidation. (a) Sample calcined under standard conditions at 400 °C for 3 h; (b) shows sample (a) further treated in O₂ at 200 °C for 3 h; (c) shows sample (a) reduced in 5% H₂/Ar at 200 °C for 2 h; and (d) shows sample (c) re-oxidised at 200 °C in O₂ for 3 h.

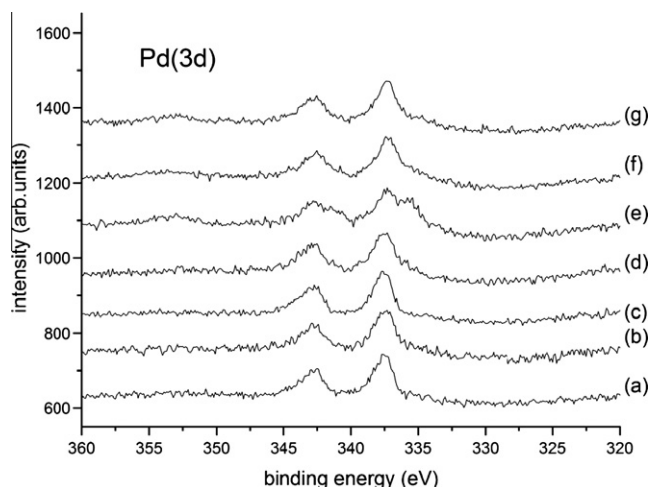


Fig. 14. Pd(3d) spectra observed for the 2.5 wt% Au–2.5 wt% Pd catalysts supported on acid pre-treated carbon with sequential reduction and oxidation. (a) calcined under standard conditions; (b) reduced in H₂/Ar at 100 °C for 1 h, (c) reduced in H₂/Ar at 110 °C for 2 h; (d) reduced in H₂/Ar at 150 °C for 2 h; (e) reduced in H₂/Ar at 200 °C for 2 h; (f) re-oxidised at 100 °C for 3 h, and (g) re-oxidised at 200 °C for 3 h.

5% H₂/Ar for 2 h, the majority of the atoms were found to have gathered up into 0.5–2.0 nm diameter metallic clusters as shown in Fig 13c. Upon re-oxidation of this reduced sample in O₂ for 3 h, the cluster morphology was largely retained (Fig. 13d), although presumably the particles were now more oxidic in character.

The corresponding Pd(3d) XPS spectra for this set of samples are shown in Fig. 14. The Cl(2p), Au(4f) and O(1s) spectra showed no significant changes in profile (see Supplemental data, Table S1). However, quantification shows that at a reduction temperature of 200 °C, the Pd/Au ratio decreases dramatically from *ca.* 3.9 to 1.3 due to an increase in the Au intensity. Re-oxidation leads to a small increase in the Pd/Au ratio to *ca.* 1.6 (see Supplemental data, Table S1). These effects are consistent with the activity of the catalyst, and as we have previously indicated, this Pd/Au ratio is important in controlling the formation of H₂O₂, since the more Pd present on the surface, the higher the catalyst activity. Hence, Pd is the crucial component of this catalyst with respect to H₂O₂ synthesis. However, as the catalysts are reduced, the amount of Pd⁰ is expected to increase. The Pd(3d) spectra were analysed to deduce the Pd²⁺ and Pd⁰ content. These were obtained through curve-fitting of the Pd(3d) spectra, although the process was complicated by the presence of the Au(4d_{5/2}) component under the Pd(3d) envelope. This is a particular problem here due to the significant surface gold content for the reduced and re-oxidised samples. Strict parameter constraints had to be used, some dependent on the estimated values for the metal-oxide binding energy shift and the magnitude of the Au(4d) spin orbit splitting. The increase in Pd⁰ is most notable for the sample in entry 5, which shows the highest hydrogenation activity; after this sample was re-oxidised, the concentration of Pd⁰ decreased as shown in Fig 15. These experiments show that the oxidation state of Pd is crucial for determining not only the initial formation of H₂O₂, but also its sequential hydrogenation. It is essential that the amount of Pd⁰ is minimised and the role of the Au and Pd²⁺ essentially is to isolate the residual Pd⁰ so that the active sites required for synthesis persist, but those for hydrogenation are minimised. As H₂O₂ hydrogenation/decomposition can be switched-off, as demonstrated by an oxidation procedure (Table 5, entry 7), then it is clear that the sites for synthesis and hydrogenation of H₂O₂ are different. This is a logical conclusion since the sites for synthesis require the associative

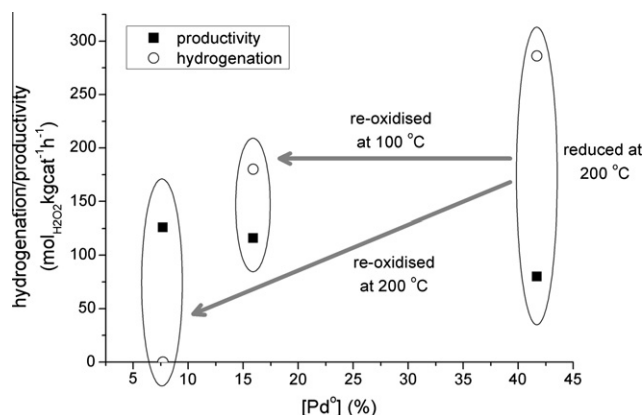


Fig. 15. Effect of surface Pd⁰ concentration on the synthesis and hydrogenation of H₂O₂.

adsorption of O₂ followed by hydrogenation, whereas the sites for hydrogenation/decomposition will break the O–O bond. Isolating Pd⁰ sites on the surface enables high rates of synthesis. It is therefore clear that the acid pre-treatment of the support presents one way of achieving this goal and that an oxidative thermal treatment presents an alternative route to this same outcome.

Acknowledgments

We acknowledge the support of the Engineering and Physical Sciences Research Council (EPSRC) of the UK (Project ATHENA) and the European Union (Project AURICAT; Contract HPRN-CT-2002-00174). We also acknowledge the financial support and technical assistance from Solvay.

Appendix A. Supplementary material

Supplementary data associated with this article can be found, in the online version, at <http://dx.doi.org/10.1016/j.jcat.2012.05.018>.

References

- [1] J.M. Campos-Martin, G. Blanco-Brieva, J.L.G. Fierro, *Angew. Chem. Int. Ed.* 45 (2006) 6962.
- [2] G. Pfeleiderer, H.J. Riedl, 2369912, 1945.
- [3] H.-J. Riedl, G. Pfeleiderer, 2158525, 1939.
- [4] V.R. Choudhary, A.G. Gaikwad, *React. Kinet. Catal. Lett.* 80 (2003) 27.
- [5] V.R. Choudhary, C. Samanta, A.G. Gaikwad, *Chem. Commun.* (2004) 2054.
- [6] V.R. Choudhary, C. Samanta, *J. Catal.* 238 (2006) 28.
- [7] V.R. Choudhary, C. Samanta, P. Jana, US 7288240, 2006.
- [8] Y.-F. Han, J.H. Lunsford, *J. Catal.* 230 (2005) 313.
- [9] Q. Liu, J.H. Lunsford, *J. Catal.* 239 (2006) 237.
- [10] Q. Liu, J.C. Bauer, R.E. Schaak, J.H. Lunsford, *Appl. Catal. A* 339 (2008) 130.
- [11] J.K. Edwards, B.E. Solsona, P. Landon, A.F. Carley, A. Herzing, C.J. Kiely, G.J. Hutchings, *J. Catal.* 236 (2005) 69.
- [12] B.E. Solsona, J.K. Edwards, P. Landon, A.F. Carley, A. Herzing, C.J. Kiely, G.J. Hutchings, *Chem. Mater.* 18 (2006) 2689.
- [13] J.K. Edwards, A. Thomas, B.E. Solsona, P. Landon, A.F. Carley, G.J. Hutchings, *Catal. Today* 122 (2007) 397.
- [14] J.K. Edwards, E. Ntainjua, N.A.F. Carley, A.A. Herzing, C.J. Kiely, G.J. Hutchings, *Angew. Chem. Int. Ed.* 48 (2009) 8512.
- [15] J.K. Edwards, B. Solsona, E. Ntainjua, N.A.F. Carley, A.A. Herzing, C.J. Kiely, G.J. Hutchings, *Science* 323 (2009) 1037.
- [16] J.C. Pritchard, Q. He, E.N. Ntainjua, M. Piccinini, J.K. Edwards, A.A. Herzing, A.F. Carley, J.A. Moulijn, C.J. Kiely, G.J. Hutchings, *Green Chem.* 12 (2010) 915.
- [17] M. Belhachemi, R. Rios, F. Addoun, J. Silvestre-Albero, A. Sepulveda-Escribano, F. Rodriguez-Reinoso, *J. Anal. Appl. Pyrol.* 86 (2009) 168.
- [18] F. Maia, R. Silva, B. Jarras, A.R. Silva, C. Freire, M.F.R. Pereira, J.L. Figueiredo, *J. Colloid Interface Sci.* 328 (2008) 314.
- [19] E. Castillejos-Lopez, D.M. Nevskaja, V. Munoz, A. Guerrero-Ruiz, *Carbon* 46 (2008) 870.
- [20] J.Y. Li, L. Ma, X.N. Li, C.S. Lu, H.Z. Liu, *Ind. Eng. Chem. Res.* 44 (2005) 5478.